Optics Letters

Proposal for detecting ring current via electron vortices

Run Wang,[1] Qingbin Zhang,[1,*] Cheng Ran,[1] Wei Cao,[1,3] and Peixiang Lu[1,2,4]

[1]School of Physics and Wuhan National Laboratory for Optoelectronics, Huazhong University of Science and Technology, Wuhan 430074, China
[2]Hubei Key Laboratory of Optical Information and Pattern Recognition, Wuhan Institute of Technology, Wuhan 430205, China
[3]e-mail: weicao@hust.edu.cn
[4]e-mail: lupeixiang@hust.edu.cn
*Corresponding author: zhangqingbin@hust.edu.cn

Received 17 January 2020; revised 1 February 2020; accepted 3 February 2020; posted 3 February 2020 (Doc. ID 388516); published 5 March 2020

In an intense circularly polarized laser field, the excitation of the atoms shows a strong dependence on the orbital helicity. The resonant excitation starting from the ground state with $m=-1$ occurs much more easily in the left-handed circularly polarized (LCP with $m=+1$) pulse than in the right-handed circularly polarized (RCP with $m=-1$) pulse. In this Letter, we numerically demonstrate that the orbital-helicity-dependent two-photon-resonant excitation leads to the photoelectron vortex pattern in the polarization plane being sensitive to the sequence of the two counter-rotating circularly polarized pulses in xenon, which enables the detection of the ring currents associated with different quantum states. These results also provide an effective way for controlling the rotational symmetry of the electron vortex.

https://doi.org/10.1364/OL.388516

The study of ionization of noble gas atoms in strong, ultrashort laser fields has led to a significant advancement of our understanding of electron dynamics on the attosecond time scale [1–4]. Despite the success, it was generally considered that the strong-field ionization (SFI) rate is only related to the modulus of magnetic quantum number $|m|$ of the target orbital [5–8]. Barth and Smirnova [9] found that the ionization rate in circularly polarized (CP) laser fields is also dependent on the sign of non-zero m. It was shown that the electron counter-rotating with respect to the laser field can be liberated more easily than the co-rotating electron. This result was later verified by Herath *et al*. [10] experimentally via measuring the strong-field sequential double-ionization yield of argon by two time-delayed near-circularly polarized laser pulses with same and opposite helicities. The orbital-helicity-dependent ionization in the CP laser field has shown the fundamental importance of understanding and controling the ionization dynamics in many atomic systems [11,12] and has opened exciting new directions, such as producing photoelectrons with spin polarization [13,14].

Besides, the application of the orbital-helicity-dependent-ionization propensity rule in Ref. [9] offers a potential tool for detecting ring currents associated with different quantum states. Kaushal *et al*. [15] theoretically studied the effects of the initial orbital momentum on the observed final angle- and energy-resolved photoelectron distributions in an angular streaking setup. To visualize the ring current experimentally, an ultrafast ionization experiment was presented in Ref. [16].

The above-mentioned experimental and theoretical works were carried out in the tunneling regime. However, the SFI of $p_{\pm}$ orbitals under the CP pulses in a deep multiphoton ionization regime was recently investigated in Refs. [17,18]. Similar rule was found, which is, that removing electrons counter-rotating with the laser pulse is strongly preferred. In addition, the helicity-sensitive excitation was also observed in the deep multiphoton ionization regime. The p_{-} electron can easily absorb N photons with $m=+1$ and be excited to $m=-1+N$ states, but it is more difficult to absorb N photons with $m=-1$ and jump to $m=-1-N$ states. Using this insight, we propose and numerically verify a new scheme to detect ring currents associated with different quantum states. Two time-delayed counter-rotating circularly polarized (CRCP) pulses have to be employed in three-photon ionization for the ground states with nonzero magnetic quantum number of xenon, which produce interfering vortex structures in the photoelectron momentum distributions (PMDs) in the polarization plane [19–23]. The cross path exists in CRCP pulses when the first pulse counter-rotates with the ground state. In this case, the electrons transit to the intermediate resonant states from the ground state by absorbing two photons in the first pulse. Then the electrons are ionized from the intermediate resonant states by one-photon absorption in the second pulse. Reversing the sequence of this pulse pair, this cross path is absent. We predict that the vortex-shaped PMDs are strongly affected by the cross path. Hence, the defined sign of the ring current can be judged according to the character of vortex patterns in PMDs in CRCP pulses with a different sequence. Furthermore, we study three-photon ionization for the superposition states composed of $p_{\pm}$ orbitals in different proportion by extracting the angular distributions for a fixed excess radial momentum from the vortex-shaped PMDs in a fixed ordering pulse pair. In this case, we find the same results for the dominant $p\pm$ orbitals. These studies can serve as an

effective way for detecting the ring currents excited in atoms and molecules in multiphoton ionization, as well as an opportunity for controlling the rotational symmetry of the electron vortex.

To calculate the PMDs, we solve the two-dimensional time-dependent Schrödinger equation (TDSE) within the length gauge and the dipole approximation using the single-active-electron (SAE) approximation for xenon in two time-delayed CRCP pulses, each of whose electric fields is given by

$$\mathbf{E}(t) = E_0 f(t)[\cos(\omega t + \Phi)\mathbf{e_x} \pm \sin(\omega t + \Phi)\mathbf{e_y}]. \quad (1)$$

The carrier envelope phases (CEPs) of the two pulses are $\Phi_1 = 0$ and $\Phi_2 = 0$, respectively. We define that a "+ (−)" sign in the y direction represents a left-handed (right-handed) circularly polarized pulse (LPH and RPH, respectively). The time delay $\Delta\tau$ between the two pulses is taken to be four optical cycles, which is large enough to ensure that the two pulses do not overlap. We solve the TDSE for an electric field $\mathbf{E}(t)$ of intensity 4×10^{13} W/cm^2 and central frequency $\omega = 0.19$ a.u. (5.17 eV), which is enough to ionize the xenon with binding energy of 0.438 a.u. by absorbing three photons. Each pulse has a temporal envelope $f(t) = \sin^2(\pi t/T)$, with the total duration $T = n_p(2\pi/\omega)$ for $n_p = 3$ optical cycles. This corresponds to the bandwidth [19] $\Delta\omega \approx 1.44\omega/n_p = 2.48$ eV, which results in the broadened photoelectron momentum distribution. Starting from the obtained initial orbitals [24,25], the TDSE equation is solved by utilizing the split-step Fourier method [26]. The time step is 0.02 a.u., and the spatial discretization is 0.1 a.u. with the dimension size of 500 a.u.

A schematic of the ionization pathways for the three-photon absorption process in CRCP pulses is depicted in Fig. 1. The ionization process for the p_- orbital in the RLCP pulse pair is shown in Fig. 1(a), which indicates that two pathways are existent: path Γ_1 indicates that the electron is ionized in the RCP pulse from the p_- orbital to the final state with $l = 4$, $m = -4$; path Γ_2 indicates three-photon absorption from the LCP pulse leading to the final states with $l = 4$, 2, $m = 2$. The corresponding ionization probability for this case is shown in Fig. 1(d), where the two plateau-like structures are caused by the first RCP pulse and the second LCP pulse, respectively. For the p_- orbital, the ionization probability in the RCP pulse is much smaller than that in the LCP pulse, which is consistent with the rule that the electrons counter-rotating with the laser pulse are strongly preferred in Ref. [17]. However, in the LRCP pulse pair, the ionization probability in the RCP pulse is much larger than that in the LCP pulse, as shown in Fig. 1(e). This abnormal phenomenon is caused by another cross path with resonant enhanced ionization in this pulse pair. Path Γ_{12} indicates the cross path in which three-photon ionization occurs by absorption of two photons from the LCP pulse and one photon from the RCP pulse, where the LCP pulse excites the intermediate resonant states of $m = +1$ [located in the yellow region in Fig. 1(b)] with energies of −2.94, −1.36, −0.78, −0.49, and −0.21 eV obtained by diagonalizing the field-free Hamiltonian [17], is followed by the RCP pulse that leads to the final states with $l = 4$, 2, 0, $m = 0$. Note that this resonant state has very long lifetimes [27], compared to the several hundred attoseconds of time delay $\Delta\tau$ employed here. As a contrast, we also discuss the three-photon ionization for the p_0 orbital, which has no cross path in both LRCP and RLCP pulses in Fig. 1(c). In these pulse pairs, the electrons are ionized from the p_0 orbital to the final states with $l = 4$, $m = \pm 3$. Figure 1(f) shows that the corresponding ionization probabilities are insensitive to the laser pulse helicity.

Through a numerical solution to the TDSE, we obtain the vortex-shaped PMDs, generated by the CRCP pulses in the polarized plane, as shown in Fig. 2. These vortex structures have been previously studied theoretically for He in the extreme ultraviolet (XUV) regime [19–21] and recently observed experimentally for potassium with 790 nm lasers [22,23]. The amplitude of ionization for the final continuum states $|l, m\rangle$ in a CP pulse can be written in the form of $M_{\Gamma_i} \propto A(E, \theta)e^{(im\phi)}$, where the $A(E, \theta)$ is proportional to the associated Legendre Polynomial $P_l^m[\cos(\theta)]$ and the spectral width ΔE [28]. Here, $E = N\omega - I_p$ denotes the variable excess energy of the electron, ϕ is the angle between the x- and y-axis in the polarized plane, and θ is the angle between the polarized plane $(x - y)$ and the z-axis. Specially, when the electron is ionized from the p_- orbital in the LCP pulse, besides the dominant $\Delta l = +1$ transitions, $\Delta l = -1$ transitions are allowed as well [22]. Note that the minor $\Delta l = -1$ transitions just have the additional contribution to the amplitude term $A(E, \theta)$, leading to variations of the vortex in the θ direction [23], and have no role on the phase term $e^{(\mathrm{im}\phi)}$ associated with the number of spiral arms. Hence, in the polarized plane at $z = 0$ $(\theta = \pi/2)$ discussed below, it is not necessary to consider this contribution to the electron vortices, when we focus on variations of the number of spiral arms. The vortex structure is formed by the interference

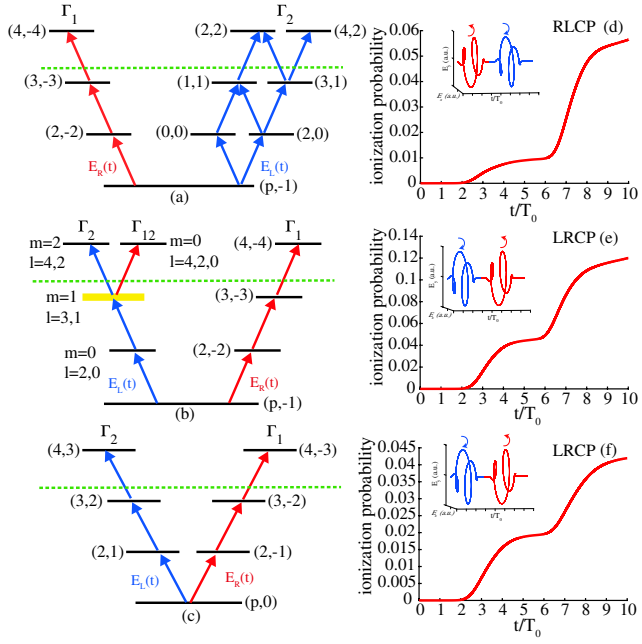

Fig. 1. Ionization schemes of xenon atom interacting with CRCP pulses, including the intermediate states and the final states in (a) and (b) for the p_- orbital, and (c) for the p_0 orbital. Here, the intermediate resonant states with $m = +1$ are marked by the yellow region in (b). The main ionization pathways are illustrated by solid arrows, where the blue and red arrows represent the photons of the LCP and RCP pulses, respectively. The blue LCP pulse is described by $\mathbf{E}_L(t)$, which exclusively drives $\Delta m = +1$ transitions. The red RCP pulse is described by $\mathbf{E}_R(t)$, which exclusively drives $\Delta m = -1$ transitions. The green dashed line represents the ionization potential I_p of 0.438 a.u. in xenon atom. On the right side, (d), (e), and (f) show the ionization probabilities corresponding to the ionization processes in (a), (b), and (c), respectively, where the insets show the laser pulses.

between the photoelectrons ionized from both paths Γ_1 and Γ_2, which can be written as $|M_{\Gamma_1}+M_{\Gamma_2}|^2 \propto A^2_{\Gamma_1}(E,\theta)+A^2_{\Gamma_2}(E,\theta)+2A_{\Gamma_1}(E,\theta)A_{\Gamma_2}(E,\theta)\cos((m_1-m_2)\phi-E\tau)$. Here, the azimuthal separation of adjacent vortex arms is $\delta\phi=2\pi/|m_1-m_2|$, and the number of spiral arms is $|m_1-m_2|$.

In Fig. 2(a), one can see that the PMD for the p_- orbital generated in the RLCP pulse pair exhibits a six-arm spiral vortex pattern with a clockwise handedness, and the vortex pattern has a sixfold rotational symmetry. Here, the six-arm spiral vortex pattern arises from the interference of two time-delayed final states with $m=2,-4$ produced by ionization paths Γ_1 and Γ_2, respectively, which is given by $|M_{\Gamma_1}+M_{\Gamma_2}|^2$. In contrast, in the resonant case in which the intermediate resonant states with $m=+1$ are populated by two-photon transition from the first LCP pulse [see Fig. 1(b)], the structure of the momentum distribution in the polarized plane changes dramatically as shown in Fig. 2(b). The PMD has a four-arm spiral vortex pattern with a counterclockwise handedness, and its rotational symmetry is broken. These results are similar to the character of the vortex patterns changed by the doubly excited states in Ref. [21]. The reason for this is that the amplitude $M_{\Gamma_{12}}$ for the ionization path Γ_{12} causes additional terms in the final interference terms. First, the interference term $|M_{\Gamma_1}+M_{\Gamma_{12}}|^2$ between the paths Γ_1 and Γ_{12} leads to a two-arm spiral vortex pattern with the same handedness as the six-arm spirals produced by the term $|M_{\Gamma_1}+M_{\Gamma_2}|^2$. Correspondingly, the interference term $|M_{\Gamma_2}+M_{\Gamma_{12}}|^2$ between the paths Γ_2 and Γ_{12} does not support a vortex pattern in the PMD because of zero delayed time occurring in the RCP pulse. Hence, the four-arm spiral vortex pattern is the result of the interplay between the terms $|M_{\Gamma_1}+M_{\Gamma_{12}}|^2$ and $|M_{\Gamma_1}+M_{\Gamma_2}|^2$. We also calculate the PMDs for the p_+ orbital in CRCP pulses with a different sequence. We find that the PMDs exhibit a six-arm spiral vortex pattern with a counterclockwise handedness in the LRCP pulse pair and a four-arm spiral vortex pattern with a clockwise handedness in the RLCP pulse pair (not shown). Hence, we can conclude that in the CRCP laser pulses with a well-defined sequence, the number of the spiral arms is different for the $p_\pm$ orbitals, which provides us the opportunity for detecting the ring current associated with the sign of m.

Furthermore, we calculate the results for the p_0 orbital ($m=0$) under the same condition for comparison. In this case, the PMDs have a six-arm spiral vortex pattern in both RLCP and LRCP pulses, as displayed in Figs. 2(c) and 2(d), respectively. In both LRCP and RLCP pulses, the electron vortices are generated by the interference of the final states with $l=4$, $m=\pm3$ [see Fig. 1(c)].

We expect that the same results can be obtained for the superposition states with different net ring currents, which are composed of the $p\pm$ orbitals in varying proportion. For this purpose, we define those initial superposition states by $\psi_i(r,t)=c_1|p,-1\rangle+c_2|p,+1\rangle \quad (c_1^2+c_2^2=1)$, where the ratio of the p_- orbital in those superposition states is $R=c_1/(c_1+c_2)$. Here, for the dominant p_- orbitals, the superposition states with $R>50\%$ possess a stationary ring current with $m=-1$, and for the dominant p_+ orbitals, the superposition states with $R<50\%$ possess a stationary ring current with $m=+1$. Specially, the superposition state with $R=50\%$ has no net ring current.

The vortex-shaped PMDs in the LRCP pulse pair for initial superposition states with $R=75\%$ and $R=25\%$ in polar representation are shown in Figs. 3(a) and 3(b). The PMDs display a four-arm vortex and a six-arm vortex (white dashed lines), respectively. To further study the disparity in the PMDs for different superposition states in more detail, we extract the angular distributions at a fixed excess radial momentum p_r from the vortex-shaped PMDs for a series of initial superposition states with R from 100% to 0, as displayed in Figs. 3(c) and 3(d). One can see that the angular distributions for the superposition states with $R>50\%$ have four lobes (spiral arms in electron

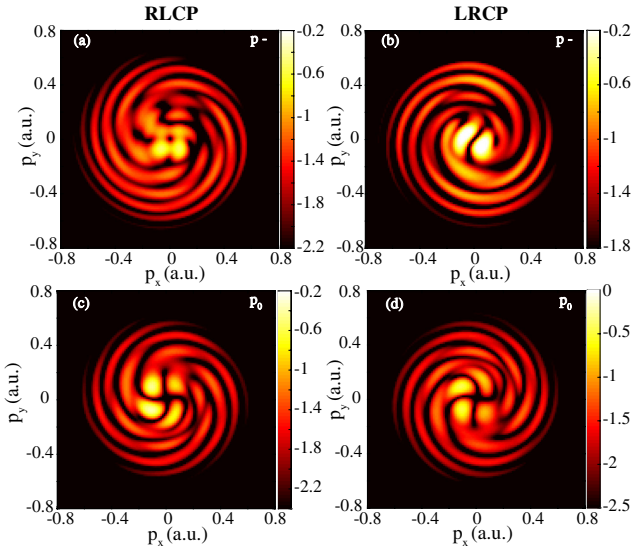

Fig. 2. PMDs for three-photon ionization of xenon in CRCP pulses. The electron vortices generated in the RLCP pulse pair for (a) the p_- orbital and (c) the p_0 orbital, and in the LRCP pulse pair for (b) the p_- orbital and (d) the p_0 orbital.

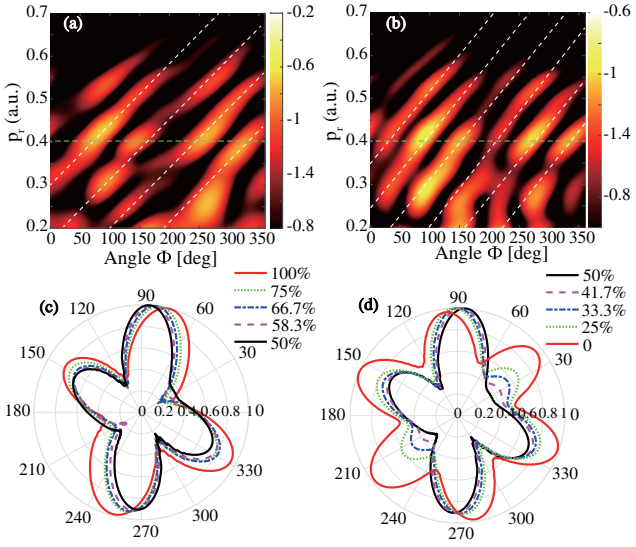

Fig. 3. Vortex-shaped PMDs in the LRCP pulse pair for different initial superposition states. (a) and (b) show the electron vortices for the initial superposition states with $R=75\%$ and $R=25\%$, respectively, in polar representation. The white dashed lines indicate the vortex arms. Angular distributions for a series of initial superposition states composed of $p_\pm$ orbitals in different proportion at $p_r=0.41$ a.u. are plotted in (c) and (d). The fixed excess radial momentum p_r is indicated by the green dashed line in (a).

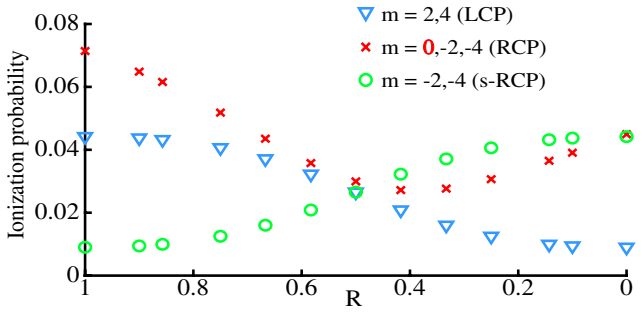

Fig. 4. Ionization probabilities for the superposition states as a function of R in different laser pulses.

vortices), and for the superposition states with $R < 50\%$ have six lobes where two lobes gradually enlarge with the increasing of the p_+ orbital. In a word, the calculated PMDs have a four-arm spiral pattern for the dominant p_- orbitals and a six-arm spiral pattern for the dominant p_+ orbitals in LRCP pulse pair. This disparity not only signifies the presence of the ring current, but it also allows us to detect its direction, by directly observing the propensity rule of the electron vortices in LRCP pulses: the spiral arm number in PMDs for the dominant p_+ orbitals is two more than for the dominant p_- orbitals, as shown in Fig. 3.

For a better understanding, the ionization probabilities for those superposition states in different laser pulses are shown in Fig. 4. In an analogy to the above discussion, in the LRCP pulse pair, the LCP pulse leads to the final states with $m = 2, 4$, and the second RCP pulse leads to the final states with $m = 0, -2, -4$, where the additional final state with $m = 0$ is generated by the cross path Γ_{12} for the p_- orbital. The single right-handed circularly polarized (s-RCP) pulse just causes the final states with $m = -2, -4$. For the dominant p_- orbitals ($R > 50\%$), the ionization probabilities in the s-RCP pulse (green circles) are smaller than those in the LCP pulse (blue triangles). However, in the LRCP pulse pair, the ionization probabilities in the RCP pulse (red crosses) are larger than that in the LCP pulse (blue triangles). This unusual phenomenon is caused by resonance-enhanced ionization in the cross path Γ_{12}. For the dominant p_+ orbitals ($R < 50\%$), the ionization probabilities in both kinds of RCP pulses (red crosses and green circles) are larger than that in the LCP pulse (blue triangles), because the resonance-enhanced ionization is absent in the LRCP pulse pair for the p_+ orbital.

In summary, by means of *ab initio* numerical solutions of the TDSE, we have investigated theoretically the PMDs of three-photon ionization of xenon by a pair of time-delayed (non-overlapping) CRCP pulses. For the p_- orbital, in RLCP pulse pair, the PMD exhibits a six-arm spiral vortex pattern stemming from a usual kind of interference between the pathways Γ_1 and Γ_2. In contrast, in the LRCP pulse pair where the intermediate resonant states with $m = +1$ are populated by two-photon transition in the first LCP pulse, the number of the spiral arms reduces to four owing to the effect of the cross pathway Γ_{12}. In analogy to the p_- orbital, for the p_+ orbital, one obtains the same results, but in the CRCP pulse with a reversing sequence. Moreover, we scan the PMDs for the superposition states with different R and abstract the angular distributions at fixed radial momentum p_r. We find that the calculated PMDs have four-arm and six-arm spiral patterns for the dominant p_- orbitals and the dominant p_+ orbitals in the LRCP pulse pair, respectively. Hence, we conclude that in the fixed sequence pulse pair, the number of the spiral arm is different for the dominant $p_\pm$ orbitals. To the best of our knowledge, our work provides a new way for detecting ring currents excited in atoms and molecules in multiphoton ionization, as well as an opportunity for controlling the rotational symmetry of the electron vortex.

Funding. National Natural Science Foundation of China (11574101, 11674116, 11774111, 11934006).

Disclosures. The authors declare no conflicts of interest.

REFERENCES

1. F. Krausz and M. Ivanov, Rev. Mod. Phys. **81**, 163 (2009).
2. A. N. Pfeiffer, C. Cirelli, M. Smolarski, X. Wang, J. H. Eberly, R. Dörner, and U. Keller, New J. Phys. **13**, 093008 (2011).
3. J. Tan, Y. Zhou, Q. Ke, M. He, J. Liang, Y. Li, M. Li, and P. Lu, Phys. Rev. A **101**, 013407 (2020).
4. K. Mi, W. Cao, H. Xu, Y. Mo, Z. Yang, P. Lan, Q. Zhang, and P. Lu, Phys. Rev. Appl. **13**, 014032 (2020).
5. G. L. Yudin and M. Y. Ivanov, Phys. Rev. A **64**, 013409 (2001).
6. Y. Zhao, Y. Zhou, J. Liang, Z. Zeng, Q. Ke, Y. Liu, M. Li, and P. Lu, Opt. Express **27**, 21689 (2019).
7. M. V. Ammosov, N. B. Delone, and V. P. Krainov, Sov. Phys. JETP **64**, 1191 (1986).
8. X. Huang, Q. Zhang, S. Xu, X. Fu, X. Han, W. Cao, and P. Lu, Opt. Express **27**, 38116 (2019).
9. I. Barth and O. Smirnova, Phys. Rev. A **84**, 063415 (2011).
10. T. Herath, L. Yan, S. K. Lee, and W. Li, Phys. Rev. Lett. **109**, 043004 (2012).
11. P. Hockett, M. Wollenhaupt, C. Lux, and T. Baumert, Phys. Rev. Lett. **112**, 223001 (2014).
12. M. Ilchen, N. Douguet, T. Mazza, A. J. Rafipoor, C. Callegari, P. Finetti, O. Plekan, K. C. Prince, A. Demidovich, C. Grazioli, L. Avaldi, P. Bolognesi, M. Coreno, M. Di Fraia, M. Devetta, Y. Ovcharenko, S. Düsterer, K. Ueda, K. Bartschat, A. N. Grum-Grzhimailo, A. V. Bozhevolnov, A. K. Kazansky, N. M. Kabachnik, and M. Meyer, Phys. Rev. Lett. **118**, 013002 (2017).
13. D. Trabert, A. Hartung, S. Eckart, F. Trinter, A. Kalinin, M. Schöffler, L. P. H. Schmidt, T. Jahnke, M. Kunitski, and R. Dörner, Phys. Rev. Lett. **120**, 043202 (2018).
14. A. Hartung, F. Morales, M. Kunitski, K. Henrichs, A. Laucke, M. Richter, T. Jahnke, A. Kalinin, M. Schöffler, L. P. H. Schmidt, M. Ivanov, O. Smirnova, and R. Dörner, Nat. Photonics **10**, 526 (2016).
15. J. Kaushal, F. Morales, and O. Smirnova, Phys. Rev. A **92**, 063405 (2015).
16. S. Eckart, M. Kunitski, M. Richter, A. Hartung, J. Rist, F. Trinter, K. Fehre, N. Schlott, K. Henrichs, L. P. H. Schmidt, T. Jahnke, M. Schöffler, K. Liu, I. Barth, J. Kaushal, F. Morales, M. Ivanov, O. Smirnova, and R. Dörner, Nat. Phys. **14**, 701 (2018).
17. X. Zhu, P. Lan, K. Liu, Y. Li, X. Liu, Q. Zhang, I. Barth, and P. Lu, Opt. Express **24**, 4196 (2016).
18. S. Kerbstadt, K. Eickhoff, T. Bayer, and M. Wollenhaupt, Adv. Phys. X **4**, 1672583 (2019).
19. J. N. Djiokap, S. Hu, L. B. Madsen, N. Manakov, A. Meremianin, and A. F. Starace, Phys. Rev. Lett. **115**, 113004 (2015).
20. J. N. Djiokap, A. V. Meremianin, N. Manakov, S. Hu, L. B. Madsen, and A. F. Starace, Phys. Rev. A **94**, 013408 (2016).
21. J. N. Djiokap and A. F. Starace, J. Opt. **19**, 124003 (2017).
22. D. Pengel, S. Kerbstadt, D. Johannmeyer, L. Englert, T. Bayer, and M. Wollenhaupt, Phys. Rev. Lett. **118**, 053003 (2017).
23. D. Pengel, S. Kerbstadt, L. Englert, T. Bayer, and M. Wollenhaupt, Phys. Rev. A **96**, 043426 (2017).
24. S. Bauch and M. Bonitz, Phys. Rev. A **78**, 043403 (2008).
25. M. Protopapas, C. H. Keitel, and P. L. Knight, Rep. Prog. Phys. **60**, 389 (1997).
26. M. Feit, J. Fleck, Jr., and A. Steiger, J. Comput. Phys. **47**, 412 (1982).
27. K. Mohamed, G. King, and F. Read, J. Phys. B **10**, 1835 (1977).
28. E. Foumouo, P. Antoine, H. Bachau, and B. Piraux, New J. Phys. **10**, 025017 (2008).